RESEARCH ARTICLE

Effect of processing conditions on morphology and mechanical damage in glass-reinforced polypropylene composite

Samia Nouira[1] | **Mohammadali Shirinbayan**[1] | **Jorge Peixinho**[1] | **Khaled Benfriha**[2] | **Tarek Hassine**[3] | **Joseph Fitoussi**[1]

[1]Arts et Metiers Institute of Technology, CNAM, CNRS, PIMM, HESAM University, Paris, France

[2]Arts et Metiers Institute of Technology, CNAM, LCPI, HESAM University, Paris, France

[3]National Engineering School of Monastir ENIM, LGM, Monastir University, Monastir, Tunisia

Correspondence
Mohammadali Shirinbayan, Arts et Metiers Institute of Technology, CNAM, CNRS, PIMM, HESAM University, F-75013 Paris, France.
Email: mohammadali.shirinbayan@ensam.eu

Abstract

This study aims to analyze the effect of processing parameters, particularly the cooling rate, on the morphology and mechanical properties of reinforced glass fiber polypropylene (GF-PP) films. To achieve the objective, a multi-scale analysis was performed to study the different morphology of neat PP and reinforced PP films obtained by controlling the thermal condition during the fabrication process. Films of PP with a thickness of about 100 μm have been prepared to observe the crystalline microstructure's formation and follow its kinetics on the scale of the spherulites. The same procedure was followed using a single glass fiber to obtain the mono-composite film of PP by controlling the interface/interphase between the fiber and the matrix. Moreover, the dependence of the damage mechanisms on the spherulite diameters and the mechanical test conditions was established. The deformation mechanisms (intra and inter-spherulitic damage) were analyzed qualitatively and quantitatively according to the controlled morphologies produced for the polymer and the composite, especially at the level of the transcrystalline phase. The results confirm that the processing parameters affect not only the width of the transcrystalline phase but also the morphology of the fiber-matrix interface. Furthermore, increasing the thickness of the transcrystalline phase exhibited remarkably higher interfacial shear strength, as demonstrated by the single fiber fragmentation test.

Highlights

- Impact of cooling rate on morphology and mechanical properties of glass fiber polypropylene (GF-PP).
- Multi-scale analysis to investigate the distinct morphologies of PP and GF-PP.
- Deformation mechanism particularly intra and inter-spherulitic damage.
- Attention to the impact on the transcrystalline phase and the fiber-matrix interface.
- Influence of transcrystalline phase thickness on interfacial strength.

KEYWORDS

composite, crystallization, damage, fragmentation, in-situ optical microscope, polymer, transcrystallinity

1 | INTRODUCTION

The quest to reduce CO_2 emissions in the automotive sector has led to a strategic shift favoring lightweight polymer matrix composites.[1–3] Replacing traditional metal components, these composites are extremely promising in weight reduction and maintaining the optimum mechanical properties essential to vehicle performance. This transition can be explained by the multi-faceted strategies adopted by the automotive industry to meet emissions reduction targets, with particular emphasis on reducing the weight of structures.

The evolution of composite materials, from their initial decorative applications to their integration into critical structural components, reflects a dynamic trajectory in various industries since the 1970s.[4] The automotive, aerospace, and civil engineering sectors have witnessed the transformative integration of composites into key components such as tailgates and shock-absorbing beams. Thanks to their exceptional energy-absorbing capacities, composites comply with safety regulations and are also the source of innovative design solutions.[5]

Among the various composite materials, those incorporating semi-crystalline thermoplastic matrices are particularly attractive because of their ease of processing and recyclability. This choice aligns with sustainability objectives while offering versatile material for engineering applications. The ease of processing and recyclability of these materials contribute significantly to their appeal, making them a preferred choice for designers and engineers in the pursuit of both performance and environmental objectives ([6,7]).

However, the effective use of composite materials depends on a nuanced understanding of their microstructure. The microstructure, which encompasses the matrix and the fiber-matrix interface, is shaped in a complex way by crystallization processes within the matrix and trans-crystallization at the reinforcement interface.[8] The outcome of these processes is influenced by a myriad of parameters, including the molecular structure of the polymer, manufacturing conditions such as cooling rate and pressure, material flow, and the incorporation of additives.

Despite the widespread adoption of composite materials, there is a critical gap in experimental knowledge concerning the response of composite microstructures to mechanical stress, particularly under various loading conditions.[9–11] This knowledge gap poses problems for engineers seeking to optimize the mechanical performance and durability of composite components.[12–14] In some cases, the absence of in situ observations based on microstructure control during deformation and damage prevents a comprehensive understanding of the effects of variations in manufacturing parameters.[15–19]

The scientific community is faced with unresolved questions, including the impact of microstructure variability on mechanical responses under monotonic loading, the influence of matrix morphology on mechanical properties and material damage, and the role of transcrystallinity in shaping composite behavior through its effects on fiber/matrix adhesion.[20–22] The identification of local microstructure-dependent damage and deformation mechanisms represents an open frontier in scientific research, requiring further exploration to unlock the full potential of lightweight polymer matrix composites in structural applications.

In summary, the structure of this study is described as follows: Section 2 provides a description of material and process-induced microstructures, and Section 3 presents the qualitative and quantitative damage analysis in pure PP samples. Section 4 gives a detailed overview of experimental procedures and damage investigation techniques in reinforced glass fiber polypropylene (GF-PP). Section 5 is devoted as a conclusion of the results of the fragmentation test under an optical microscope.

2 | EXPERIMENTAL PROCEDURE

2.1 | Material

Commercial granules of isotactic polypropylene were supplied by Chemieuro France (PPH 4060), with a melting flow index of 3 g/10 min and a melting density of 0.905 g.cm^{-3}. The percentage of atacticity of the polymer used was estimated at 1%. The fibers utilized were E-glass fibers with an average diameter of approx. 10 µm, supplied by Zhengtong Chemical Industry. The fibers were rinsed with acetone then placed in deionized water under ultrasound for 20 minutes in order to eliminate the industrial sizing. The fibers were dried in a vacuum oven at 60°C for 12 h.

2.2 | Specimen preparation

Thin PP and GF-PP films were prepared by hot compression molding. A PP film with a thickness of 100 μm was fixed by adhesive tape on the flat surface of a Teflon sheet. A single fiber has been manually separated from a bundle. Subsequently, the two ends of the fiber were glued to the PP sheet to keep it as straight as possible along the longitudinal axis of the PP sheet. The second sheet of PP was placed above the first one with the fiber. The compression molding was set at 190°C. The temperature of two steel plates is controlled with thermocouples. When the desired temperature is reached, the assembly of GF-PP is transferred between the heated plates of the press unit. A pressure of 20 bars was applied to the sample for 90 seconds. Then the specimen is cooled to room temperature for a few minutes.

Then, the microstructures of the samples were monitored and controlled using a hot-stage (Linkam HMS600) under nitrogen. Afterward, the sample specimen was heated above its melting temperature to 206°C for 5 min to dissociate any crystal and then cooled down to 25°C at different cooling rates. This step allows us to have information on the non-isothermal crystallization of the material.

2.3 | Polarized optical microscopy (POM)

To investigate the morphology of the interphase between the PP matrix and the glass fiber, we used a Nikon LV N100 microscope equipped with polarized filters. This instrument enabled precise observation a recorded the evolving interphase during the non-isothermal crystallization process. Through this methodological lens, we delved into the special and temporal aspects of the interphase, investigating how varying crystallization conditions influenced its development.

2.4 | Single fiber tensile strength test

A mono-composite with a fiber gauge length of 20 mm, was held in a micro-traction machine, designed and fabricated in PIMM laboratory.[23] The micro traction machine, which was developed in the laboratory, is coupled with the microscope. The machine consists of a frame, an electric motor, a 20 dN force cell, one fixed and one movable jaw, gears, a slide and a ball screw. The traction plate support can be mobilized in the frame plane by two microscope axes, either automatically or manually. Each axis is equipped with a position sensor, to identify the viewing area on the sample during deformation. Control of the distance between the two jaws is ensured by the system: motor, gears, and ball screw, which moves the movable jaw. The speed of this movement varies between 10 and 5000 μm/s. The measured force is taken as the resistance experienced by the fiber as it is pulled into the polymer matrix.

3 | INFLUENCE OF CRYSTALLINE MORPHOLOGY ON POLYMER DAMAGE

3.1 | Qualitative analysis

The observations presented in this section show the evolution and the deformation of spherulites constituting the microstructure. The different colors in the images of Figures 1 and 2 are related to the objectives and the working distance used on the microscope. Additionally, dark areas appearing in the images do not represent a discontinuity in the microstructure, in fact, all the spherulites touch each other and their presence is related to the observation plane used.

In the following paragraph, a qualitative comparison of different microstructures has been reported. The description is detailed in three parts to describe the damage phenomenon for the three microstructures presented previously. We found three distinct cooling rates, each giving rise to a unique microstructure characterized by the average diameter of spherulites. Specifically, we denote these microstructures as PP10, PP50, and PP100, signifying spherulite diameters of 10, 50, and 100 μm, respectively.

Figure 1 shows the condition of spherulites during an in-situ tensile test. It is a microstructure resulting from a cooling rate equal to $20°C.min^{-1}$, drawn at a rate equal to 0.1 mm/min. No defects were observed in this simple up to an elongation of 4%. For a strain of 6%, the deformation seems to be homogeneous in the microstructure. For 9% strain, a deformation of the core of the spherulite is observed, it starts at the borders of the crystal and its entities and passes toward the equatorial parts of the spherulites.

This deformation is similar to undulations that continue to extend to the heart of the spherulite. This state is illustrated with the white dashed lines in images of Figure 1 which indicate the edges of the center of the spherulite.

The deformation in the equatorial zones where the crystalline lamellae are perpendicular to the axis of solicitation is a proof of localization of deformation at the polymer level. At the level of the flow plateau, at 100%

deformation, the spherulitic structure starts to disappear until the structure. At this stage, any spherulitic texture turns into a fibrillar structure as shown in Figure 2.

In addition, at the breakage for a more advanced percentage of deformation, we noticed a channel of deformation of the equatorial part that involves a separation in two of the spherulitic.

Figure 2A shows the deformation of the PP10 film. Indeed, the deformation starts from the intra-spherulitic part and propagates in the crystalline lamellae at the inter-spherulitic boundaries passing through a fibrillar structure and reaching failure. After a thorough examination of the material damage, we find a homogeneous deformation up to plastic deformation for PP10. These observations suggest that the uniform plastic deformation results from a homogeneous activation of plastic processes at the local scale of spherulites. This feature confirms the strong cohesion of the material at the inter-spherulitic boundaries. The absence of cracks is then a major characteristic of PP10.

It should be noted that for small spherulites, the core and polar regions of the deformed crystalline features appear at a higher altitude than the equatorial regions. This observation can be translated by the effective transmission of stresses between adjacent spherulites which has a primary role to have an affine deformation at the microscopic scale. Furthermore, the topological singularity of spherulitic boundaries becomes less distinct with increasing plastic deformation, and may even disappear in several parts of the material. The observations of uniform deformation of PP10, also suggest the presence of uniform fragmentation. This phenomenon cannot be described in this study because it is difficult or even impossible to see the fragments of the crystalline lamellae under an optical microscope. According to Weynant et al.,[24] it has been suggested that the activation of the inter-lamellar slip in stacks with an oblique orientation could cross the other lamellar stacks of opposite orientation which favors the inter-lamellar crystal slip. As already mentioned, PP has different plastic capacities depending on the plastic size, so a comparison is made between large and small spherulites. A cavitation phenomenon was predominant in this microstructure during the plastic plateau.

Furthermore, we studied the deformation of PP100 films with large spherules, as shown in Figure 2B. In a tensile test with low speeds, small deformation at the equatorial channels was observed in a tensile test at low speeds. Micro-cracks were detected at the boundaries between the spherulites. At these locations, a fibril structure oriented along the tensile direction starts to appear as soon as the linearity is lost at the tensile curve.

In the polar zones of spherulites, several black lines are observed at the lips of the crystalline entities. These zones characterize the beginning of the fragmentation phenomenon. This phenomenon then spreads until the matrix rupture which will be faster than PP10 and PP50.

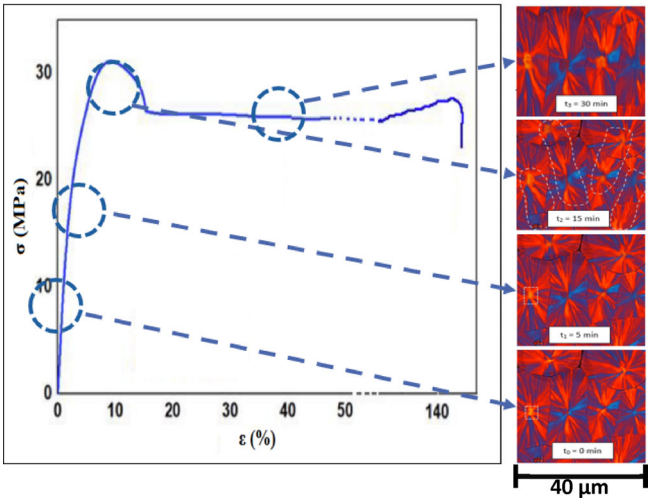

FIGURE 1 The different stages of a tensile test of PP10. Each image is taken at different times (and strains), the white dashed lines indicate deformed center of the spherulite. The strain axis is on the vertical direction.

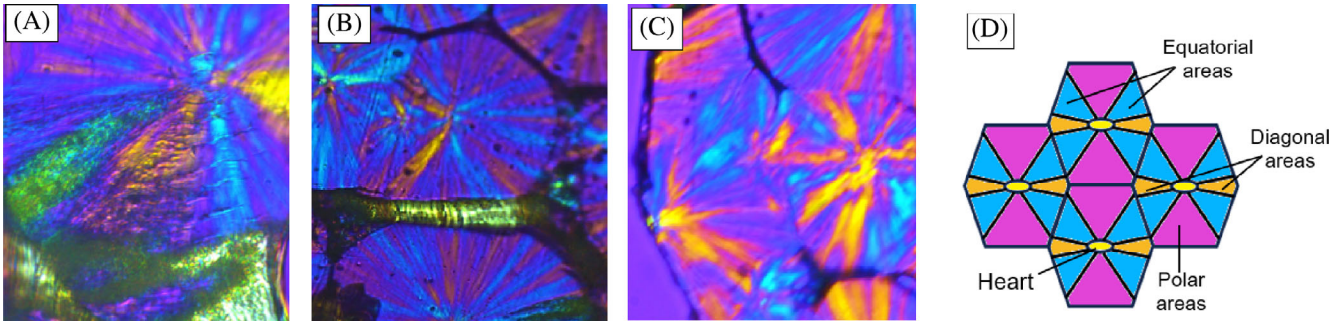

FIGURE 2 State of the microstructure during a load for different films respectively: (A) represents PP10, (B) shows PP100, (C) PP50, and (D) Schematic illustration.

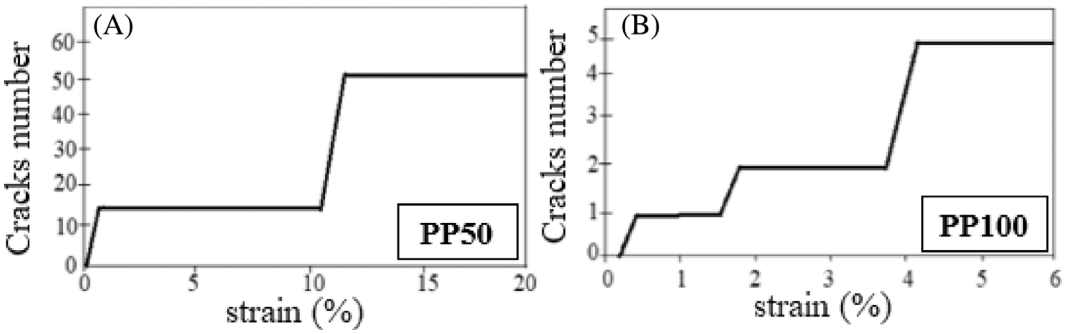

FIGURE 3 Number of cracks of PP50 and PP100 films.

At the beginning of the solicitation, the damage in PP100 films is remarkable between the spherulites then it spreads in the equatorial regions of spherulites with good preservation of the entirety of the crystallite entity in the polar parts. This observation confirms the fact that the driving force of cavitation lies in the rigidity of the crystalline lamellae which confirms the increase of Young's modulus compared to other microstructures. The multiplication of cracks is then observed at the level of the borders of the large spherulites which favors the rupture of the material. For this category of films, we can confirm the presence of perfectly inter-spherulitic damage. This observation can confirm the low percentages of deformation found for a low cooling rate. In this case, the damage to the material depends on the entanglement of the amorphous parts between the spherulites. For the PP50 films, Figure 2C shows pictures of the state of the material during an in-situ tensile test.

In a microstructure characterized by spherulites with a diameter of 50 μm, there are indications of both inter- and intra-spherulitic damage. A deformation at the boundaries of the spherulites starts to reach the rupture of the spherulites at the core. Additionally, the presence of cracks is observed, leading to a distinct separation among crystalline entities. Notably, a fibrillar structure was not observed in this particular film type.

3.2 | Quantitative analysis: Number of cracks as a function of the deformation

The phenomenon of cracking was observed for films with spherulitic diameters between 50 and 100 μm. Therefore, in this paragraph the number of cracks counted at low deformations for the films PP50 and PP100 is presented in Figure 3. Crack counting was performed by in-situ examination of the recorded images during the loading test. The procedure was repeated on multiple samples using the threshold function of the imageJ software.

Comparing the two microstructures, we note the presence of a very large number of cracks for PP50 compared to PP100. This difference can be related to the number of spherulites formed in each microstructure.

This work presents the different plastic deformation and damage processes of polypropylene with spherulites of different sizes, namely PP100, PP5O, and PP10. Different observations show that a difference of a few tens of microns in the size of spherulites have a huge effect on the development of plastic processes. Indeed, large spherulites show cracks and cavitation leading to a more brittle behavior while small spherulites have a homogeneous fragmentation leading to a high plastic deformation.

A common feature between small and large PP spherulites is the continuity of plastic deformation in the inter-spherulitic regions. This feature defines the transfer of stresses across the spherulitic boundaries despite the structural heterogeneity in this area.

To enhance the depth of our exploration into the influence of microstructure on the mechanical behavior of the polymer, the ensuing section encapsulates the derived mechanical properties. So, the modulus of elasticity and strain at break were assessed across various microstructures. Thus, the determination of those parameters for several microstructures is illustrated in Figure 4. The presence of a critical cooling rate, ϕ_c, range between 1 and 5°C/min is observed, with a significant change in the initial modulus marked by this rate. The diversity and complexity of the factors influencing the mechanical behavior of the semi-crystalline polymer are highlighted by the variation in mechanical properties.

4 | TRANSCRYSTALLIZATION PHENOMENON WITH A SINGULAR FIBER IN THE PP MATRIX

The objective of this part is to study the effect of manufacturing conditions, in particular the speed of

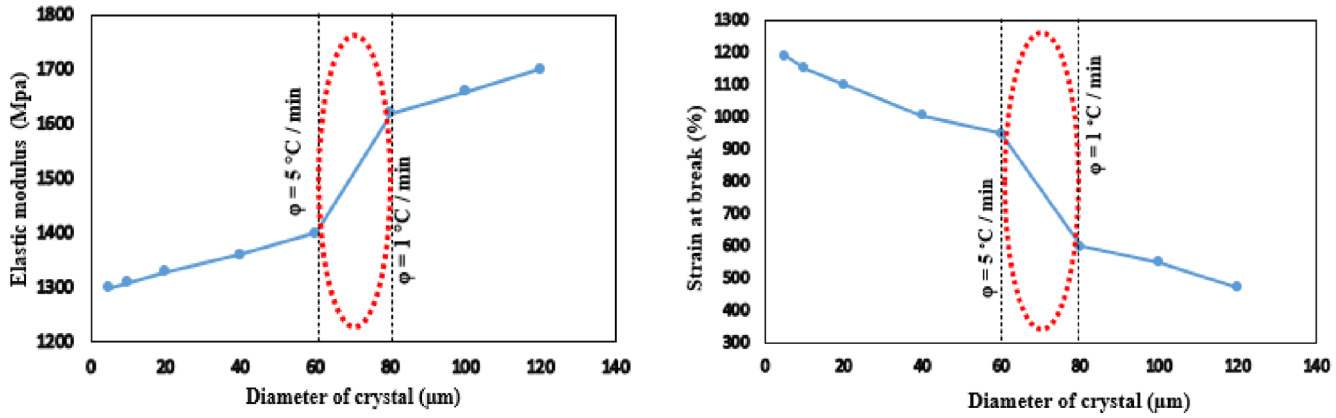

FIGURE 4 Effect of cooling rate on mechanical properties.

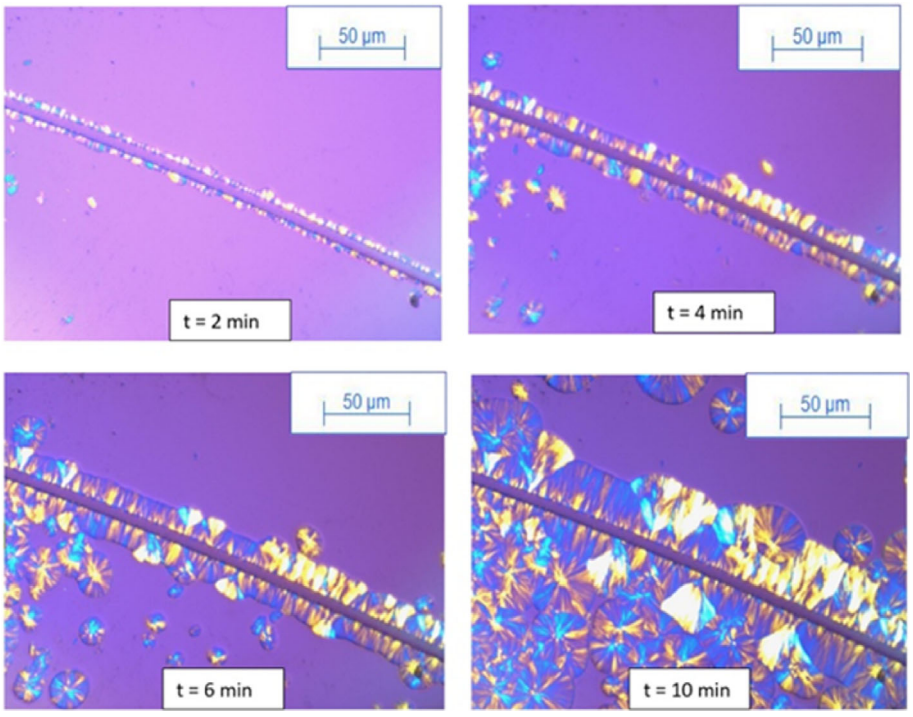

FIGURE 5 The dtages of transcrystalline phase formation on fiber surface.

crystallization of the polymer on the morphology and properties of a mono-composite. This study will allow observing the formation of the transcrystalline phase (T_c), at the edge of the fiber embedded in the polypropylene, as a function of time and cooling rate.

4.1 | Qualitative analysis

4.1.1 | Formation of a transcrystalline around the fiber

The stages of transcrystalline layer (T_c) formation during non-isothermal cooling from the molten state are investigated in our study. Photographs were captured at various intermediate times. The development of crystalline entities perpendicular to the fiber axis is indeed observed. The illustration of the steps in the formation of the interface around a glass fiber impregnated in a PP matrix at a constant cooling rate of 1°C/min is presented in Figure 5.

A common feature between small and large PP spherulites is the continuity of plastic deformation in the inter-spherulitic regions. This feature defines the transfer of stresses across the spherulitic boundaries despite the structural heterogeneity in this area.

The germination on the surface of the matrix fiber can be detected. The diameter of these crystalline entities increases with time, thereby augmenting the thickness of the T_c layer. Delayed germination at the matrix level is

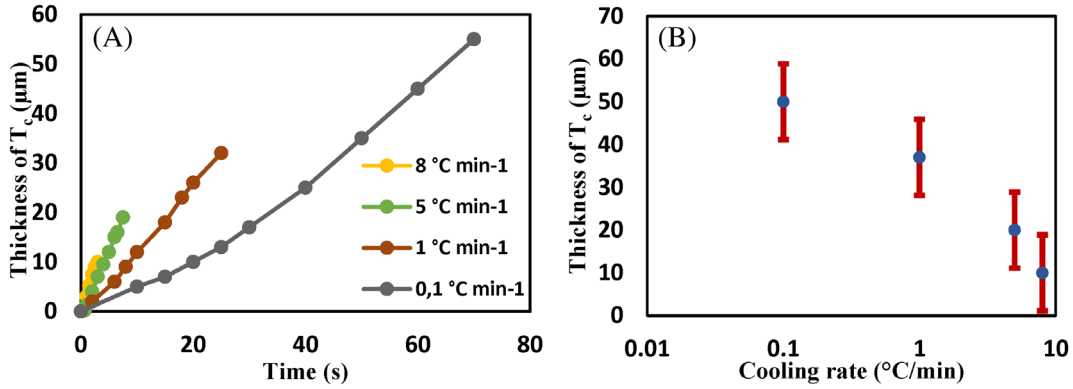

FIGURE 6 Evolution of the thickness of the transcrystalline part as a function of the time and the cooling rate.

observed on the same figures. The development of the microstructure is then completed over time as the spherulites of the matrix come into contact with those of the T_c, preventing their growth. The evolution of the T_C thickness as a function of time was revealed for different cooling rates as shown in Figure 6.

The crystallization process unfolds as anticipated, initiating on the fiber surface and subsequently progressing within the matrix. Elevating the cooling rates accelerates the rapid development of the transcrystalline segment, with the thickness of Tc constrained by the growth rate of matrix spherulites. Notably, at cooling rates ranging from 0.1 to 1°C/min, the formation of T_c layers proceeds at a sluggish pace, resulting in the most uniform and thickest layers. Consequently, the nucleation density at the fiber surface surpasses that in the matrix. The presence of a foreign body enhances germination and transcrystalline entity growth, resulting in limited germination in the matrix due to the lower cooling rate. This, in turn, augments the available space in the polymer melt. Subsequently, T_c layers uniformly expand before encroaching upon the polymer spherulites.

At higher cooling rates, specifically in the range of 5 to 30°C/min, a thinner and less uniform T_c layer becomes apparent. This is attributed to a significant increase in seed formation within the matrix, driven by elevated supercooling. The proliferation of numerous spherulites in the molten matrix impedes the growth of the transcrystalline layer.

Figure 7 shows the different values found for each cooling rate. Thus, a clear decrease in the thickness of the transcrystalline part by increasing the cooling speed is observed.

In situ observations were conducted to scrutinize the final state of the microstructure in the mono-composite. These observations unveiled noticeable differences in thicknesses, providing valuable insights into the variations within the composite's structural characteristics.

4.1.2 | Effect of cooling rate on transcrystalline morphology

In this section, a depiction of the distinction in morphologies of the transcrystalline components developed at different cooling rates was crafted.

Two cooling rates, 1 and 5°C/min, were selected for this analysis. Between these two speeds, an alteration in the morphology of the transcrystalline (T_C) structure was observed.

During non-isothermal cooling, two distinct morphologies of the transcrystalline part were identified. For cooling rates equal to or greater than 5°C/min, crystalline entities of the α-form manifested on the fiber surface. Conversely, at very low cooling rates around 1°C/min, both α and β crystalline forms were observed. According to existing literature, this disparity is attributed to the nucleation phenomenon. A perfectly heterogeneous nucleation results in a transcrystalline part exhibiting cylindrical growth with both α and β crystalline entities. Conversely, homogeneous self-nucleation on the fiber surface leads to the exclusive observation of monoclinic crystalline forms. Figure 8 exemplifies the contrast between these observations.

These observations reveal a lighter color for the β crystalline forms, indicative of their lesser stability and compactness compared to the α form. The term "frustrated" is aptly applied to the β form due to its structurally more disordered nature than the α form.

In this section, the qualitative study of the impact of the cooling rate on the in-situ development of the transcrystalline part under the optical microscope was undertaken. In the subsequent section, the quantitative exploration of the cooling rate's influence on the

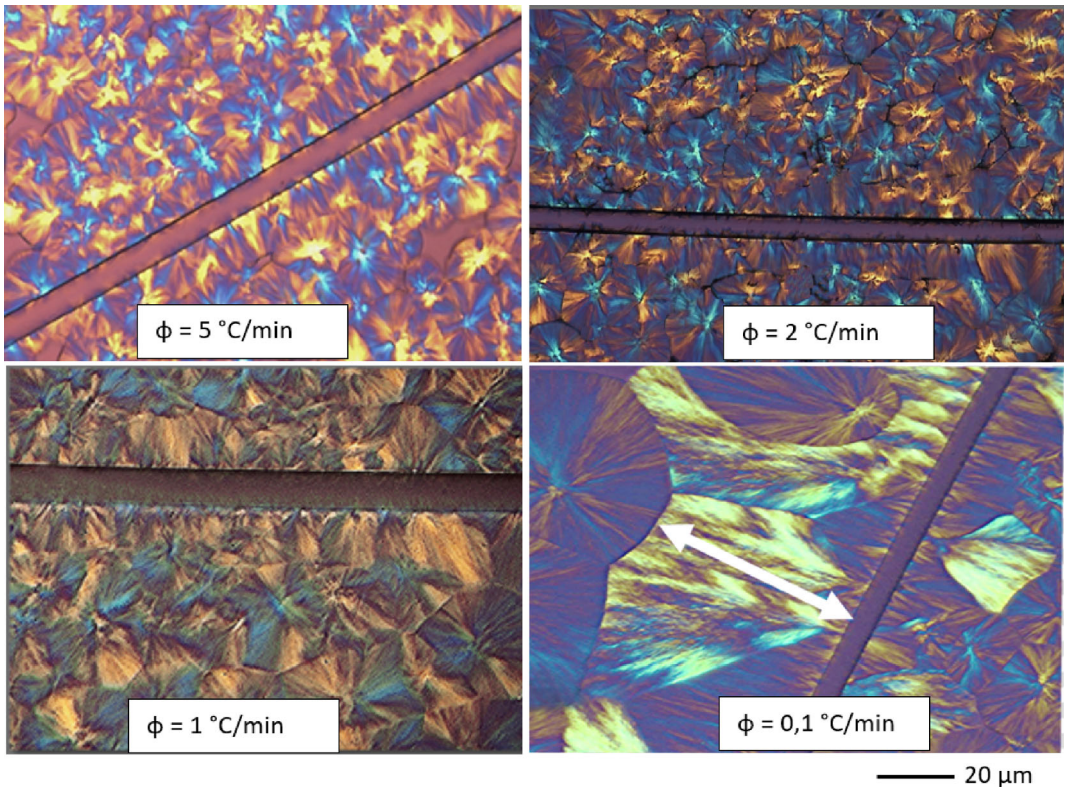

FIGURE 7 The different microstructures depending on the cooling rate.

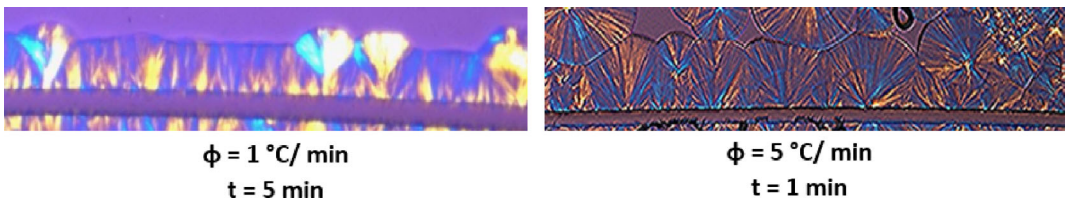

FIGURE 8 The different morphologies observed at the fiber/matrix interface as a function of the cooling rate.

mono-composite's mechanical properties will be conducted.

4.2 | Quantitative analysis of the damage of PP/long glass fiber at different cooling rates

4.2.1 | Transverse tensile behavior of unidirectional composite materials: Experimental insights

To investigate the influence of the transcrystalline phase, a tensile test was conducted with the fiber positioned perpendicular to the direction of loading. This experimental approach facilitated the observation of fiber-matrix interface decohesion and provided insights into the impact of the transcrystalline (T_c) layer on the material's behavior and damage.

The response of the mono composite to tensile stress, applied perpendicular to the fiber direction, was examined at cooling rates of 5 and 30°C/min, as illustrated in Figure 9. This analysis allows for a comprehensive understanding of the material's mechanical response under the specified conditions, shedding light on the role played by the transcrystalline phase in influencing the observed behaviors, as shown in Figure 9.

After these observations, a high cooling rate was noted, distinguished by a transcrystalline part not discernible at the microscope scale, and it was observed that the damage to the fiber matrix occurs at the interface. At this scale, no damage at the matrix level was observed. Conversely, for a low cooling rate, where the transcrystalline part is observable, the damage during the tensile test

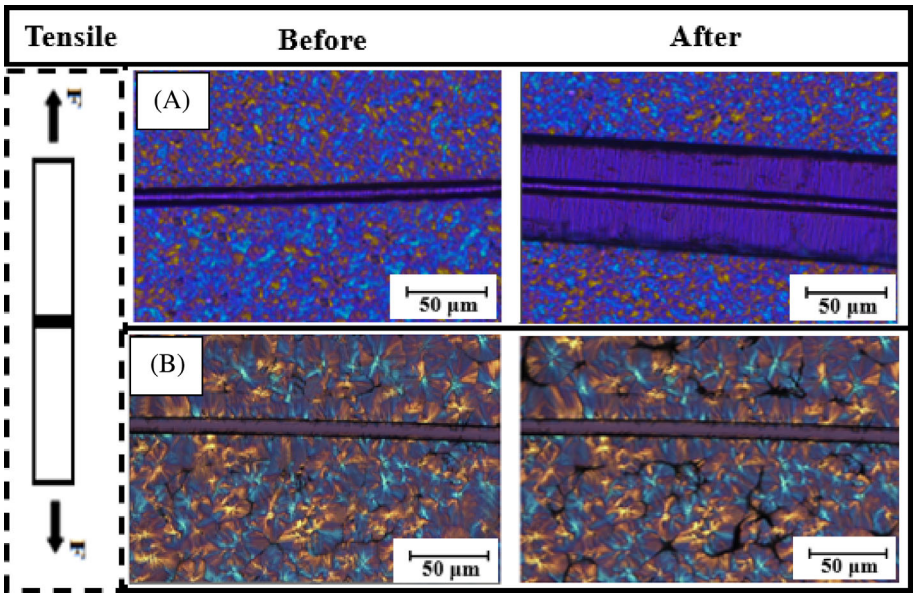

FIGURE 9 Microstructural changes pre- and post-tensile test: A comparative analysis at cooling rates of respectively 30°C/min in figure (A) and 10°C/min figure (B).

is situated at the matrix level. This positioning at the matrix level is a direct consequence of the influence of the presence of the transcrystalline phase on the damage. Consequently, the stress is transferred to the matrix by the transcrystalline phase.

4.2.2 | Fragmentation phenomenon in unidirectional composites: Unraveling longitudinal tensile effects

Monocomposite damage is studied by applying stress in the same direction as the fiber. The fragmentation method described below is therefore employed. The fragmentation test is one of the most frequently used methods for characterizing adhesion between fiber and matrix, as well as for assessing the interfacial shear strength of the composite, denoted τ. This value indicates the degree of load transfer for a fiber/matrix system.

In this test, a sample with a single fiber embedded in the middle of a polymer matrix is subjected to stress. As the stress is applied, the load is transferred from the matrix to the fiber by shear at the interface. When the stress reaches its limit in the fiber, the latter fragments. This phenomenon continues until saturation is reached, and the fiber fragments cannot withstand their limit stresses due to the shortening of the load-transferring part. This length is called the saturation length (L_s) or critical length. It represents the maximum value that can be stressed to cause the material to break.

The critical fiber length is estimated using the following equation:

$$L_s = \frac{4}{3}\overline{L}, \tag{1}$$

with $\overline{L}$ is the average length of the fragments.

The interfacial shear strength τ is then calculated using the Kelly-Tyson equation[25]

$$\tau = \frac{\sigma_f d}{2L_s}, \tag{2}$$

with σ_f is the tensile yield stress determined for a fragment of critical length L_s and d is the fiber diameter.

The identification of the length of the fiber fragments is very important for an accurate estimation of the interfacial shear strength. On the other hand, these breaks may be mixed with other defects in the material. Therefore, we perform in-situ observations under an optical microscope during a tensile test.

In Figure 10, the influence of cooling rates, specifically the effect of transcrystallinity on the damage of a monocomposite, is examined. To explore this effect, an in-situ analysis was performed on various samples subjected to different manufacturing parameters. A clearer observation of the transcrystalline region is facilitated by a lower cooling rate, enabling the scrutiny of crack initiation at the spherulite scale.

In a microstructure controlled at a cooling rate of 1°C/min, crack initiation at the fiber-matrix interface is observed at low deformation within the transcrystalline region. This initiation progresses toward the fiber, leading to subsequent fragmentation. The emergence of additional fragments along the fiber is revealed with increased stress.

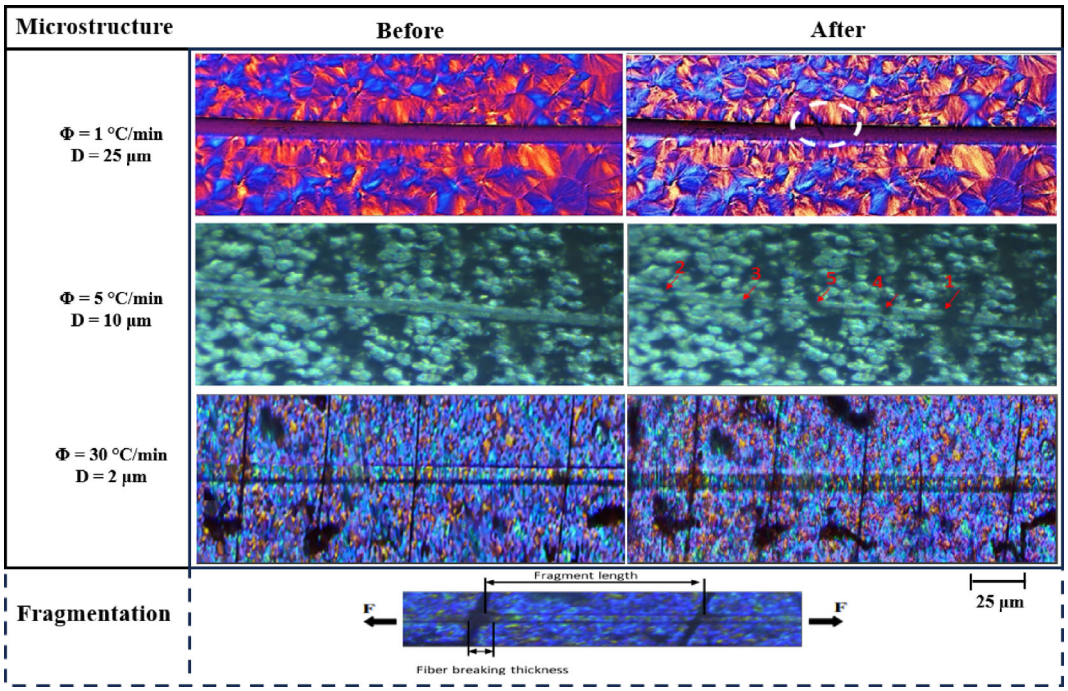

FIGURE 10 Crack propagation for different microstructures.

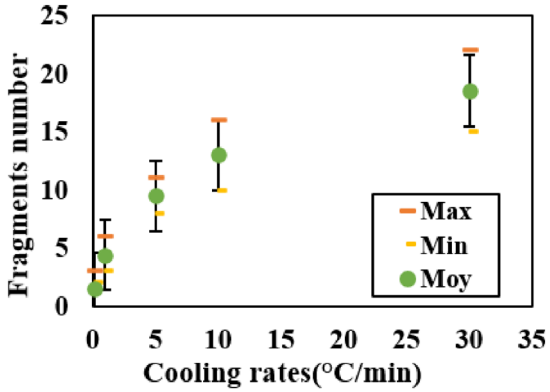

FIGURE 11 Fragmentation count versus cooling rate in transcrystallinity impact on monocomposite damage.

Similarly, for a sample cooled at 5°C/min, distinct stages of fragmentation are evident, consistently observed at the transcrystalline region. These in-situ tests also facilitate the quantification and monitoring of fragment appearances.

Moreover, the same figure depicts a sample cooled at a rate of 30°C/min. In this instance, the transcrystalline phase remains undetectable, yet fragment appearances are observed. With increased deformation, matrix cracks become apparent. The cohesion of the latter with fragments at the fiber-matrix interface is noteworthy.

This investigation presents a quantitative analysis of the correlation between transcrystallinity and fragment count during mechanical loading. The study aims to understand how the transcrystalline effect affects the resulting fragmentation under applied stress. The outcomes are illustrated in Figure 11, providing a comprehensive representation of the quantitative impact of transcrystallinity on fragment count throughout the loading process. It is worth noting that increasing the speed from 0.1 to 30°C/min results in a sevenfold increase in the number of fragments.

The fibers are completely submerged in the polymer melt, and the fragmentation count is performed along the entire length of the 20-micron fibers.

These observations also contribute to determining the interfacial strength of the material under varying cooling conditions. Additionally, the mechanical properties of the mono-composite were assessed through in-situ tensile tests at different cooling rates. An incremental reduction in the modulus of elasticity was observed with increasing cooling rates. Conversely, a noticeable rise in the material's maximum stress occurred as the thickness of the transcrystalline phase decreased. The corresponding values for each cooling speed are presented in the following Table 1. The table also provides the counting of fragments, which systematically increases with the cooling rate. The critical length between cracks along the fiber and perpendicular to its axis. Finally, the interfacial shear strength calculated from the Kelly-Tyson equation (2) is found to decrease with the cooling rate.

Furthermore, Table 1 provides insight into the values of the interfacial shear strength (τ). Notably, the

TABLE 1 The mechanical properties and results of fragmentation tests of the different microstructures.

Cooling rate (°C/min)	Film thickness (μm)	Young modulus (MPa)	Yield stress (MPa)	Counting of fragments			Critical length (mm)	Interfacial shear strength, τ (MPa)
				max	min	moy		
0.1	100 ± 10	2620 ± 50	42	3	2	1.5	0.95 ± 0.5	6.3
1	100 ± 5	2500 ± 50	51	6	3	4.4	2.0 ± 0.4	3.9
5	95 ± 5	2430 ± 50	57	11	8	9.5	2.4 ± 0.25	2.5
10	90 ± 5	2350 ± 20	68	16	10	13	2.6 ± 0.5	2.3
30	80 ± 2	2280 ± 20	78	22	15	18.5	3.0 ± 0.3	2

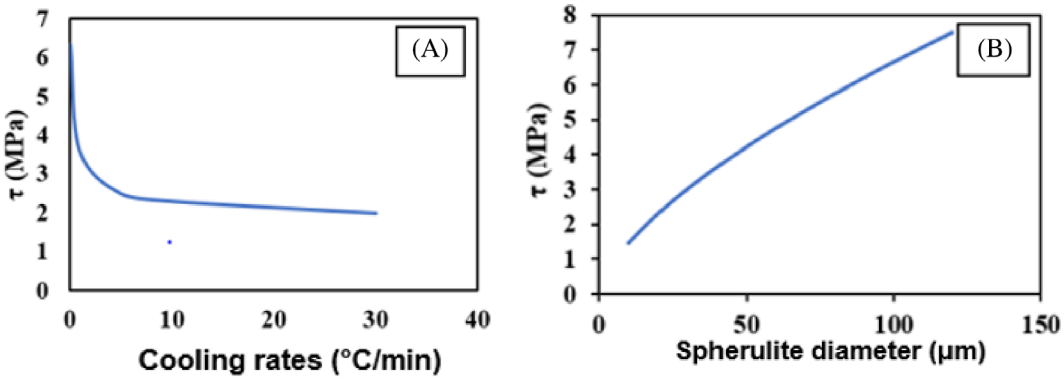

FIGURE 12 Evolution of interfacial shear strength as a function of cooling rate.

thickness of the crystalline phase exerts a discernible influence on the fiber/matrix interface. An evident trend emerges, showcasing an increase in τ with the augmentation of the transcrystalline phase thickness, as presented in Figure 12A. Remarkably, there is a notable 200% surge in interfacial shear strength with the escalation of the cooling rate from 0.1 to 30°C/min. The presence of this phase can be construed as yielding a positive impact on interfacial adhesion. This can be attributed to the transcrystalline part's effect on altering residual stress at the interface, subsequently influencing the viscoelastic response of the matrix.

To further investigate the variation in interfacial shear strength concerning microstructure, the study explored an augmentation in shear strength concurrent with an increase in spherulitic sizes, as shown in Figure 12B. An exponential relationship underscores this correlation.

$$\tau = 0.32e^{0.66}. \quad (3)$$

5 | CONCLUSION

The work carried out in this article has shown that the cooling rate of the material has an effect not only on the morphology of the microstructure, but also on the damage behavior. It was observed that damage occurs intra-spherulites with the appearance of a fibrillar structure for small spherulites. In contrast, damage occurs in the inter-spherulitic parts for large spherulites, with the appearance of micro-cracks and the absence of any fibrillar transformation of the microstructure. Furthermore, alterations in microstructure have an impact on the mechanical properties of the material. Increasing the spherulite diameter results in a slight increase in stiffness, while also causing a significant decrease in the percentage of deformations. This study also examines the impact of cooling rate on the transcrystalline section in the presence of a fiber. It has been demonstrated that embedding glass fibers in an isotactic polypropylene matrix is an optimal system for investigating transcrystallinity. The creation, development, and ultimate size of the transcrystalline phase can be readily regulated during production. In this area and at low cooling rates, morphologies of the fiber/matrix interface have been identified, resulting in the emergence of β-shape and α-shape, which impact adhesion strength. To comprehend the impact of transcrystalline phase thickness, we conducted in-situ mechanical tests under an optical microscope. Two types of tests were performed. Firstly, a uniaxial force was applied to a mono-composite with a fiber perpendicular to the loading direction. We observed matrix

deformation during the test for films with a thick transcrystalline phase. Conversely, for films without this component, damage occurred at the fiber/matrix interface. The results indicate that the presence of transcrystallinity enhances adhesion between the matrix and reinforcement. Fragmentation tests were conducted in the second part, which confirmed the increase in interfacial shear strength with an increase in the thickness of the transcrystalline part. These results support the findings of the previous test. Controlling the microstructure to obtain a transcrystalline part enhances fiber/matrix adhesion. This allows industrialists to avoid chemical treatments to modify the fiber's surface state and favor nucleation sites.

AUTHOR CONTRIBUTIONS

Samia Nouira, Mohammadali Shirinbayan, and Joseph Fitoussi collaborated on developing the initial idea. Jorge Peixinho, Khaled Benfriha, Tarek Hassine, and Joseph Fitoussi analyzed the results, contributed to drafting the manuscript, and authored the article. Additionally, Samia Nouira, Mohammadali Shirinbayan, Jorge Peixinho, Khaled Benfriha, Tarek Hassine, and Joseph Fitoussi collectively revised the English language and ensured proper formatting of the article.

CONFLICT OF INTEREST STATEMENT

The authors declare that they have no conflicts of interest.

DATA AVAILABILITY STATEMENT

The authors declare that the data and the materials of this study are available within the article.

ORCID

Mohammadali Shirinbayan https://orcid.org/0000-0002-2757-8529

REFERENCES

1. Arif MF, Saintier N, Meraghni F, Fitoussi J, Chemisky Y, Robert G. Multiscale fatigue damage characterization in short glass fiber reinforced polyamide-66. *Compos Part B Eng*. 2014; 1(61):55-65.
2. Mattner T, Wrensch M, Drummer D. Shear behavior of woven and non-crimp fabric based thermoplastic composites at near-processing conditions. *Compos Part B Eng*. 2020;15(185): 107761.
3. Lotz B, Wittmann JC, Lovinger AJ. Structure and morphology of poly(propylenes): a molecular analysis. *Polymer*. 1996;37(22): 4979-4992.
4. Subadra SP, Yousef S, Griskevicius P, Makarevicius V. High-performance fiberglass/epoxy reinforced by functionalized CNTs for vehicle applications with less fuel consumption and greenhouse gas emissions. *Polym Test*. 2020;1(86):106480.
5. Sunil Kumar MR, Schmidova E, Konopík P, Melzer D, Bozkurt F, Londe V. Fracture toughness analysis of automotive-grade dual-phase steel using essential work of fracture (EWF) method. *Metals*. 2020;10(8):1019.
6. Jun X, Zhu L, Nie Y, et al. Advances and challenges of self-healing elastomers: a mini review. *Materials*. 2022;15(5993): 5993.
7. Percec V, Xiao Q. From organic chemistry to chemical biology via macromolecules with Hermann Staudinger. *Giant*. 2020; 1(4):100036.
8. Weynant E, Haudin JM, G'Sell C. Plastic deformation and solid-phase transformation in polybutene-1. *J Mater Sci*. 1982; 17(4):1017-1035.
9. Fischer C, Drummer D. Crystallization and mechanical properties of polypropylene under processing-relevant cooling conditions with respect to isothermal holding time. *Int J Polym Sci*. 2016;15(2016):e5450708.
10. Cho K, Li F, Choi J. Crystallization and melting behavior of polypropylene and maleated polypropylene blends. *Polymer*. 1999;40(7):1719-1729.
11. Xia XF, Zhang JH, Fan JM, Jiang QL, Xu SA. Effect of functionalization on non-isothermal crystallization behavior of polypropylene. *Int J Polym Anal Charact*. 2016;21(8): 697-707.
12. Bessard E, de Almeida O, Bernhart G. Etude et modélisation de la cinétique de cristallisation du PEEK lors de refroidissements isothermes et anisothermes. In: AMAC, ed. *17èmes Journées Nationales sur les Composites (JNC17) [Internet]*. Poitiers-Futuroscope; 2011:105 https://hal.archives-ouvertes.fr/hal-00598154
13. Boni S, G'Sell C, Weynant E, Haudin JM. Microscopic in situ observation of the plastic deformation of polybutene-1 films under simple shear. *Polym Test*. 1982;3(1):3-24.
14. Khellafi H, Chikh B, Bouchouicha B. Contribution à l'étude de la quantification de l'endommagement et détermination des facteurs influençant le processus de nucléation des cavités dans les polymères. 2016.
15. Yang X, Wu Y, Wei K, Fang W, Sun H. Non-isothermal crystallization kinetics of short glass fiber reinforced poly (ether ether ketone) composites. *Materials*. 2018;11(11):2094.
16. Ozawa T. Kinetics of non-isothermal crystallization. *Polymer*. 1971;12(3):150-158.
17. Lanyi FJ, Wenzke N, Kaschta J, Schubert DW. On the determination of the enthalpy of fusion of α-crystalline isotactic polypropylene using differential scanning calorimetry, X-ray diffraction, and Fourier-transform infrared spectroscopy: an old story revisited. *Adv Eng Mater*. 2020;22(9):1900796.
18. Tian J, Yu W, Zhou C. Crystallization behaviors of linear and long chain branched polypropylene. *J Appl Polym Sci*. 2007; 104(6):3592-3600.
19. Gole J, Stout JD, Burda C, Lou Y, Chen X. Highly efficient formation of visible light tunable TiO2-XNx photocatalysts their transform at the nanoscale. *J Phys Chem B*. 2004;1:108.
20. Luo S, Wei L, Sun J, et al. Crystallization behavior and optical properties of isotactic polypropylene filled with α-nucleating agents of multilayered distribution. *RSC Adv*. 2019;10(1): 387-393.
21. Peng W, Sun F, Liang Y, et al. Exploring the effects of MXene on nonisothermal crystallization and melting behavior of

β-nucleated isotactic polypropylene. *Polymers*. 2021;13(21): 3815.
22. Douwe-Wiebe M. Structure-property relationships in isotactic polypropylene: the influence of chain architecture and nucleation on crystallization, morphology and mechanical properties. *Phys Rev Lett*. 2003.
23. Nouira S, Hassine T, Fitoussi J, Shirinbayan M, Gamaoun F, Tcharkhtchi A. Non-isothermal crystallization kinetics and its effect on the mechanical properties of homopolymer isotactic polypropylene. *J Polym Res*. 2021;29(1):26.
24. Weynant E, Haudin JM, G'Sell C. In situ observation of the spherulite deformation in polybutene-1 (modification I). *J Mater Sci*. 1980;15(11):2677-2692.
25. Aliotta L, Lazzeri A. A proposal to modify the Kelly-Tyson equation to calculate the interfacial shear strength (IFSS) of composites with low aspect ratio fibers. *Compos Sci Technol*. 2020;20(186):107920.